Edge localized modes and the pedestal: A model based on coupled peeling–ballooning modes[a)]

P. B. Snyder[b)]
General Atomics, P.O. Box 85608, San Diego, California 92186-5608

H. R. Wilson
EURATOM/UKAEA Fusion Association, Culham Science Centre, Abingdon, Oxon OX14 3DB, United Kingdom

J. R. Ferron, L. L. Lao, A. W. Leonard, T. H. Osborne, and A. D. Turnbull
General Atomics, P.O. Box 85608, San Diego, California 92186-5608

D. Mossessian
Massachusetts Institute of Technology, Cambridge, Massachusetts 02139

M. Murakami
Oak Ridge National Laboratory, Oak Ridge, Tennessee 37831

X. Q. Xu
Lawrence Livermore National Laboratory, Livermore, California 94550

(Received 29 October 2001; accepted 14 November 2001)

A model based on magnetohydrodynamic (MHD) stability of the tokamak plasma edge region is presented, which describes characteristics of edge localized modes (ELMs) and the pedestal. The model emphasizes the dual role played by large bootstrap currents driven by the sharp pressure gradients in the pedestal region. Pedestal currents reduce the edge magnetic shear, stabilizing high toroidal mode number (n) ballooning modes, while at the same time providing drive for intermediate to low n peeling modes. The result is that coupled peeling–ballooning modes at intermediate n ($3<n<20$) are often the limiting instability which constrains the pedestal and triggers ELMs. These modes are characterized in shaped tokamak equilibria using an efficient new numerical code, and simplified models are developed for pedestal limits and the ELM cycle. Results are compared to several experiments, and nonideal MHD effects are briefly discussed. © *2002 American Institute of Physics.* [DOI: 10.1063/1.1449463]

I. INTRODUCTION

The high confinement regime known as H-mode is a promising operational regime for a tokamak fusion device. H-mode is characterized by the development of a transport barrier, which forms a ''pedestal'' in the density and temperature profiles, in the outer region of the plasma, just inside the magnetic separatrix. Steady state operation in H-mode is generally accompanied by the bursty edge perturbations known as edge localized modes (ELMs). ELMs have the beneficial effect of transporting density and impurities across the H-mode pedestal region; however, large ELMs can produce high peak heat loads on the divertor plates which may be intolerable in a fusion reactor. Perhaps even more important, ELMs limit the pedestal pressure gradient, and, together with edge transport, can directly limit the pressure and temperature at the top of the pedestal (i.e., the ''pedestal height''). Both theory-based transport models and experimental observation indicate a strong dependence of the overall confinement in the core of a magnetic fusion device on the pedestal height. Achieving at least a modestly high pedestal appears necessary for successful operation of currently envisioned next step fusion devices, and determining under what conditions a high pedestal may be achieved in conjunction with tolerable ELMs requires a detailed, predictive understanding of ELM physics.

ELMs are short, repetitive perturbations of plasma in the edge region, which occur during H-mode and VH-mode operation and lead to particle and energy loss. A rich variety of ELM phenomena has been observed, and are well described in recent reviews.[1,2] We focus primarily on developing a model of the large and small ELMs, which occur in the high pedestal pressure regimes of interest to next step devices, and provide *de facto* limits on the pedestal height achievable in experiments.

The theory of ELMs has been an active area of investigation over the past decade, and comprehensive reviews of both ELM[1–5] and pedestal[6,7] theory and experimental results are available. In this paper, we present a model of ELMs and constraints on the pedestal based on coupled peeling–ballooning modes, compare the model to experiment, and

[a)]Paper UI1 6, Bull. Am. Phys. Soc. **46**, 323 (2001).
[b)]Invited speaker. Electronic mail: snyder@fusion.gat.com

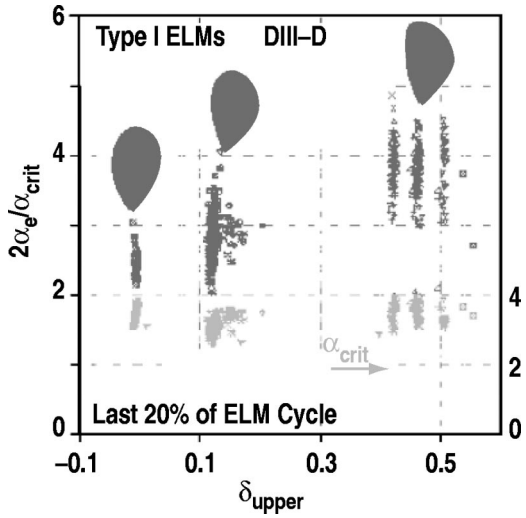

FIG. 1. Normalized edge pressure gradient (α) averaged over the last 20% of the ELM cycle as a function of the upper triangularity of the plasma shape. Also plotted is the critical normalized pressure gradient for ideal ballooning stability (α_{crit}), calculated in the absence of edge J_{bs}.

discuss its implications. Section II gives a brief discussion of peeling modes and the role current plays in the pedestal region. Section III describes the new numerical code, ELITE, which has been developed to allow efficient, detailed study of peeling–ballooning modes. In Sec. IV we describe our model of the ELM cycle and pedestal limits, including proposed physics mechanisms for the ELM trigger, and the limitations imposed on the pedestal gradient and height by peeling–ballooning modes. Section V compares the model with experimental results from several tokamaks, and Sec. VI briefly discusses the impact of nonideal magnetohydrodynamic (MHD) effects such as diamagnetic stabilization.

II. PEELING MODES AND THE ROLE OF CURRENT IN THE PEDESTAL

The magnetic fluctuation signatures, proximity to the ideal ballooning limit, and short time scale for ELM growth suggest a relationship between ELMs and ideal MHD instabilities that has been explored by numerous authors.

However, simple models based entirely on pressure driven high-n ideal ballooning modes, without consideration of the impact of edge current, appear to be ruled out by experiment. While the high-n ideal ballooning limit does correspond well to the observed type I ELM threshold in some regimes, recent experiments with high edge spatial resolution diagnostics indicate that the ideal ballooning limit can be substantially exceeded, and that observed pressure gradient limits do not scale as expected from ideal ballooning theory (see, for example, Refs. 8–10). Figure 1 shows the results from a scan of the plasma triangularity in DIII-D,[11] indicating both that the ideal ballooning limit can be substantially exceeded at high triangularity, and that the strong scaling of the pressure gradient limit with triangularity is not predicted by ideal ballooning theory.[8] Similar scaling of the normalized pressure gradient with triangularity has been observed on other tokamaks.

Incorporating the impact of edge current and finite n can overcome the above difficulties and lead to more comprehensive models of ELM stability. The sharp pressure gradients in the H-mode pedestal can drive strong bootstrap currents which play a complex dual role in the stability picture. On the one hand, edge current provides a source of free energy which drives external kink or "peeling" modes in the edge. On the other hand, edge current reduces the magnetic shear ($\hat{s}$) in the pedestal, which stabilizes high-n ballooning modes, and increases the MHD pressure gradient threshold. A further complication is introduced by the coupling between peeling and ballooning modes which occurs at finite n.

Finite edge current can drive external modes localized near the plasma edge. These modes were dubbed "peeling" modes by Frieman *et al.*,[12] and localized criteria for peeling stability have been given by Lortz,[13] Wesson,[14] and Connor *et al.*[15] Peeling modes are found to be most unstable when a rational surface is located just outside the plasma, minimizing the stabilizing influence of magnetic perturbations in the vacuum. In this limit, for large mode number, a necessary stability criterion can be written[15]

$$\sqrt{1-4D_M} > 1 + \frac{2}{2\pi q'} \oint \frac{J_\parallel B}{R^2 B_p^3} dl, \tag{1}$$

where D_M is the Mercier coefficient ($D_M < 1/4$ is the Mercier stability criterion[16]), $J_\parallel$ is the current density along the magnetic field $\mathbf{B}$, q' is the derivative of the safety factor with respect to the poloidal flux Ψ, B_p is the poloidal field, and dl is the poloidal arc length element, with all quantities evaluated at the plasma surface. Finite (positive) edge current is destabilizing, magnetic shear is stabilizing, and the pressure gradient is also stabilizing, as it increases the amplitude of D_M, which is generally negative. Equation (1) provides useful insight into peeling mode stability; however, it is a necessary, but not sufficient condition for peeling stability, as it considers only modes which are radially localized on the scale of the distance between rational surfaces, and furthermore it neglects the stabilizing contribution of the vacuum energy. At finite mode number, particularly for low n modes in shaped geometry, multiple poloidal harmonics couple and a more detailed treatment is required to calculate stability thresholds.

Studies focusing on the higher end of the n spectrum have emphasized the impact of second stability to ballooning modes, and of coupling of peeling and ballooning modes that occurs at finite n.[15,17–20] Figure 2[18] illustrates several important features of peeling–ballooning coupling via stability calculations in $\hat{s}-\alpha$ geometry,[21] with the addition of a "magnetic well factor" $d_M = D_M \hat{s}^2/\alpha$ which models the effects of shaping and finite aspect ratio. In the $n \to \infty$ limit, the peeling and ballooning thresholds can both be obtained from simple 1-D calculations,[15] and these are shown as the "pure peeling" and "pure ballooning" curves in Fig. 2(a). Note that the peeling mode is driven unstable by edge current [$\hat{s} = 2(1 - J_a/\langle J \rangle)$, where J_a is the current density on the outermost flux surface, and $\langle J \rangle$ is the average current density in the plasma] and stabilized by finite α as expected [Eq. (1)], and

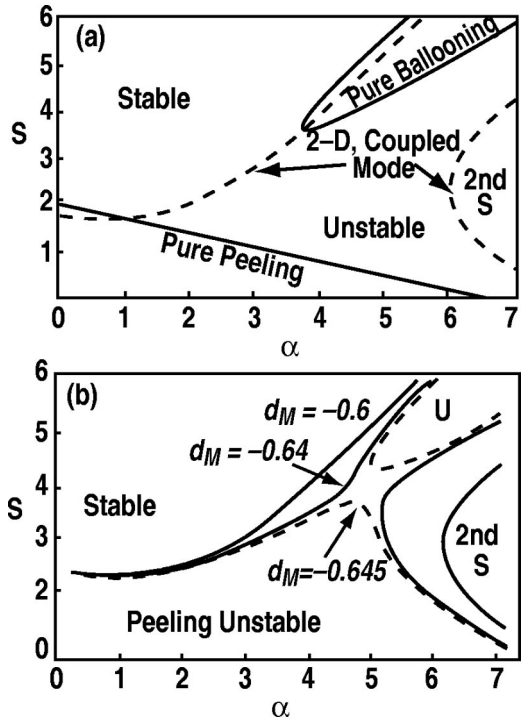

FIG. 2. The marginal stability contours in $\hat{s}-\alpha$ space for (a) the $n=\infty$ pure peeling and pure ballooning modes, as well as the $n=20$, $d_M=-0.6$ 2D coupled peeling–ballooning mode and (b) a sequence of curves for the $n=20$ 2D coupled mode, with $d_M=-0.6,-0.64,-0.645$, showing second stability access reopening at the deepest well ($d_M=-0.645$).

that a wide stable path to the second stable region exists, between the pure peeling and pure ballooning unstable regions. However, at finite values of n ($n=20$ is shown), the peeling and ballooning modes couple and can close off access to the second stability region, as shown by the ''2D coupled mode'' curves in Fig. 2(a). Increasing the magnetic well decouples the modes and reopens second stability access as shown in Fig. 2(b). The strength of the peeling–ballooning coupling is a function of n, and the second stability gap opens more easily for higher n modes. As the magnetic well deepens (i.e., shaping improves), the edge stability transitions rapidly from a regime in which essentially no n's have second access ($n\gtrsim 50$ will generally be stabilized by finite Larmor radius effects), to a regime in which all $n\gtrsim 10$ have access to second stability.

Including current in studies of the pedestal leads to a separate dependence of MHD stability on density and temperature, rather than just pressure, because of the strong collisional dependence of the bootstrap current. Important implications of this will be discussed further in Sec. IV.

III. THE ELITE CODE

Analysis of peeling–ballooning modes in simple geometry suggests that stabilization of high-n ballooning modes by magnetic shear, destabilization of peeling modes by current, and peeling–ballooning coupling combine to imply that intermediate-n coupled peeling–ballooning modes are often the most unstable MHD modes in the pedestal. Furthermore, the stability of these modes is expected to be a strong function of cross section shape, as well as pressure and current profiles.

To develop a quantitative model, and allow for detailed comparisons with experiment, a highly efficient tool able to characterize pedestal stability over a broad range of n and a wide, multidimensional space of pedestal parameters is needed. To this end, we have developed the Edge Localized Instabilities in Tokamak Experiments (ELITE) MHD stability code. ELITE employs an extension of classical ballooning theory to incorporate the surface terms which drive peeling modes, and carries the expansion through two orders in $1/n$ for accuracy at intermediate to high $n\gtrsim 5$. A further expansion is carried out in poloidal harmonics (m). At high n, a large number of poloidal harmonics are important, however each harmonic tends to be localized around its rational surface(s). ELITE employs a windowing technique, allowing it to retain a relatively small number of m's at each radial location for numerical efficiency. The analytic expansion procedure, and further details of the code are described in a companion paper.[22] ELITE outputs not only stability thresholds, but also growth rates, and poloidal and radial mode structures. ELITE has been successfully benchmarked against the MISHKA compressionless MHD code[23] for $5<n<50$,[22] and against the GATO code[24] as described in the following section.

IV. ELM AND PEDESTAL MODEL

Peeling modes become unstable at large J_{ped}, but are stabilized by increasing p'_{ped}. High-n ballooning modes are unstable at large p'_{ped} at low J_{ped}, and coupled peeling–ballooning modes are unstable at large p'_{ped} and large J_{ped}. Increased shaping (i.e., higher D_M) decouples the peeling and ballooning modes and leads to stability limits at higher p'_{ped}, J_{ped} and lower values of n.

These stability limits can be quantified using the ELITE code in conjunction with low-n stability codes such as GATO. One approach is to fix the density/temperature ratio and the pedestal width, and vary the pedestal pressure gradient, while calculating the bootstrap current self-consistently. Following this procedure for different cross section shapes allows us to further quantify the ''working model'' of ELMs developed on DIII-D.[4,9] Figure 3 shows the stability thresholds calculated by GATO and ELITE for an equilibrium based on a low squareness DIII-D discharge, for which large ELMs and high p' are observed in the experiment. For this case, the nominal ballooning limit (the $n=\infty$ limit calculated with the edge current forced to zero) is $p'=3.1\ \mathrm{Pa\,Wb^{-1}\,Rad}$, and pressure gradients exceeding this limit by factors of 2 to 3 are observed in the experiment, in reasonable agreement with the predicted stability limit, imposed by $n=10$ peeling–ballooning modes at $p'\sim 8\ \mathrm{Pa\,Wb^{-1}\,Rad}$. Note that good agreement in both predicted stability threshold and mode structure is achieved between GATO and ELITE in their region of overlap ($4\leqslant n\leqslant 10$), providing a successful benchmark of the two codes.

Figure 3 also provides a demonstration that the concept of second stability, developed from simple analysis in $\hat{s}-\alpha$

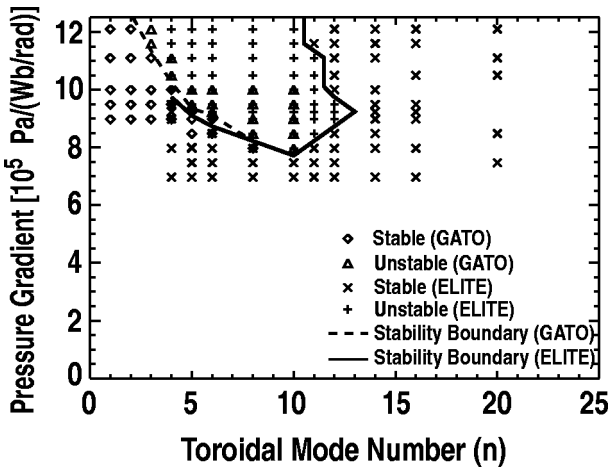

FIG. 3. Stability threshold in p',n space calculated using the GATO and ELITE codes.

geometry, carries over to shaped 2D global equilibria. In the presence of the large bootstrap current, which reduces magnetic shear, high $n \gtrsim 15$ modes are stabilized, and remain stable at pressure gradients well in excess of the high-n ballooning limit that obtains in the absence of bootstrap current ($p' = 3.1$ Pa Wb^{-1} Rad).

In general, the density and temperature can vary independently, allowing for multiple self-consistent values of the pedestal current at a given p'. To explore the two-dimensional pedestal parameter space in this more general case, we construct a set of up–down symmetric D-shaped equilibria, chosen to resemble Joint European Torus (JET)[25] plasmas, with major radius $R = 3$ m, elongation $\kappa = 1.6$, triangularity $\delta = 0.3$, and fixed shape hyperbolic tangent temperature and density profiles. The current profile is calculated self-consistently including Pfirsh–Schlüter, diamagnetic, bootstrap, and ohmic contributions, accounting for collisionality corrections. Stability is then calculated for a range of modes, $5 < n < 31$. The stability boundary for this range of modes, and radial eigenmode structures of the limiting instabilities are shown in Fig. 4. Because the shape of the profiles

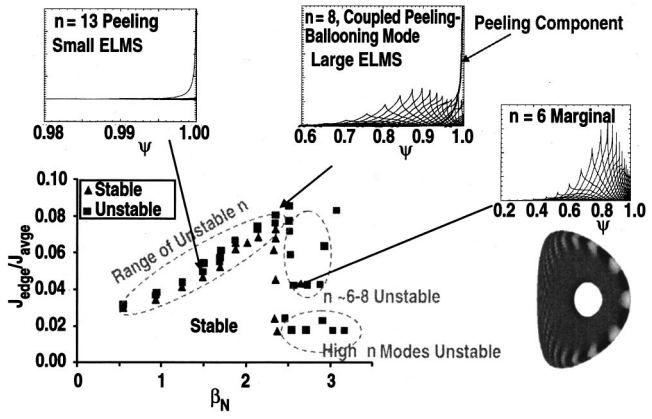

FIG. 4. Stability boundary in J, β_N space for the range $5 < n < 31$ for JET-like equilibria with $\kappa = 1.6$, $\delta = 0.5$. The radial eigenmode of the limiting instability in different regimes is also shown, along with a contour plot of the 2D structure of an $n = 6$ peeling–ballooning mode.

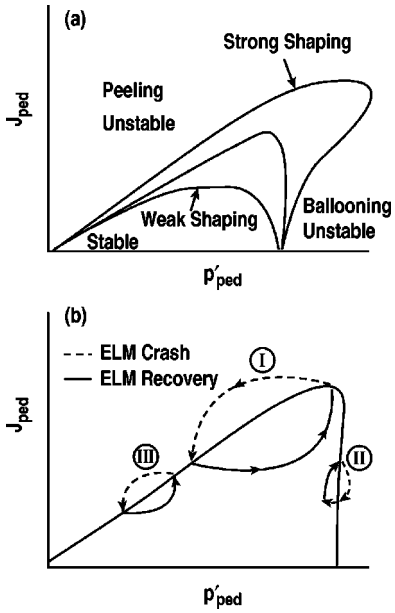

FIG. 5. (a) Schematic diagram of stability limits in p'_{ped}, $J_{\mathrm{ped}}/\langle J \rangle$ space, for a variety of cross section shapes. (b) Proposed simplified model of small and large ELM cycles.

is fixed, the pressure limit can be described equivalently in terms of p' or p, and here is given by the normalized $\beta_N = \beta a B/I$, where I is the total plasma current, and the plasma $\beta = 8\pi p/B^2$. For these equilibria, second stability to high-n ballooning modes is possible at high current, however this access is cut off by intermediate $n = 6-8$ peeling–ballooning modes as shown. Stability boundaries calculated in this fashion set limits on the pedestal height at a given width, and the calculated radial extent of the mode structure in various regimes is employed in our ELM model. Furthermore, we note that, largely because of the strong collisionality dependence of the bootstrap current, there is a monotonic relationship between the pedestal current, and the pedestal temperature (T_e) in the regime of interest. Hence it is possible to recast Fig. 4 in β_N, T_e space, and calculate limits on the pedestal temperature itself imposed directly by MHD stability. For the above case, this yields a T_e limit of ~ 2.6 keV at $\beta_N \sim 2$. Increasing triangularity to $\delta = 0.5$ increases this limit to ~ 3.2 keV.

These stability calculations suggest a model of ELMs in which peeling–ballooning instabilities provide the trigger, and ELM size correlates with the radial depth of the most unstable mode. The stability limits imposed by coupled peeling–ballooning modes can be envisioned schematically as in Fig. 5(a). The location in p', J space at the time the ELM is triggered will also contribute to its dynamics, and it is possible to postulate semiquantitative models of various types of ELM cycle. At least three types of MHD-driven ELM cycle can be envisioned for this type of stability boundary, as illustrated schematically in Fig. 5(b). In each case, power flowing from the core causes the pedestal gradients to rise between ELMs on a transport time scale, with (mostly bootstrap) current generally rising more slowly toward its steady state value. The cycle labeled "III" will oc-

cur at low density and low input power, such that the current rises to exceed the peeling limit well before the pressure gradient reaches the ballooning limit. These ELMs are expected to be small, both because the peeling modes triggering them have narrow mode structures, and because they occur at low pedestal height. The ELM frequency is expected to decrease with input power, because the pressure gradient will rise more quickly, stabilizing the peeling mode. Hence this cycle provides a model for the low density variety of Type III ELMs (high density Type III ELMs are likely driven by resistive modes beyond the scope of ideal MHD analysis). At higher power and low density, cycle ''I'' will occur, generating large ELMs both because the relatively low-n peeling–ballooning modes have a broad radial structure, and because the initial pedestal pressure collapse will leave the pedestal in the unstable domain until the current relaxes to a much lower value. This cycle's frequency will increase with input power, and it provides a model for large type I ELMs. Finally, at large input power, where the total steady state current at the pressure limit does not exceed the peeling limit ($J_{\mathrm{tot}}<J_{\mathrm{peel}}$), cycle ''II'' occurs. This can occur either at high density, where high collisionality leads to a low J_{bs} (leading to a model of small type I ELMs), or it can occur at somewhat lower density when the peeling limit is high due to strong shaping or large magnetic shear. This cycle is expected to yield relatively small ELMs because both the high-n ballooning modes which are most unstable at low current, and the intermediate-n modes most unstable for high-q high δ type-II ELM cases, tend to have narrow mode structures, and because the pressure loss immediately following the ELM crash returns the pedestal to a stable region of parameter space.

Note that in the above stability studies, the density and temperature profile shapes, and therefore the pedestal width, have been held fixed. Stability limits will in general be a function of this width, which is likely determined by a complex interplay of transport, stability, and atomic physics. Stability itself can place constraints on the pedestal width at a given gradient, as finite-n modes are sensitive to the pedestal height as well as the local gradient. Study of these stability based constraints on the pedestal width and their integration with transport constraints is an important direction for future work.

V. COMPARISON WITH EXPERIMENT

Recent advances in high resolution pedestal diagnostics allow for detailed comparisons of the model with a range of experimental measurements.

General trends in pedestal stability with shape have been found to agree with experimental observations.[8,9] ELITE calculations such as those shown in Fig. 3, allow further quantification of such comparisons, and are found to agree with observed pressure gradient limits in strongly shaped discharges, as discussed in the preceding section.

To provide a direct confrontation of the stability-based model with experiment, we present first a case study, following the time evolution of DIII-D VH-mode shot 97887 and evaluating the feasibility of intermediate-n peeling–ballooning modes as a trigger for observed ELMs. We then briefly discuss additional comparisons on the JT-60U[26] and Alcator C-Mod[27] tokamaks.

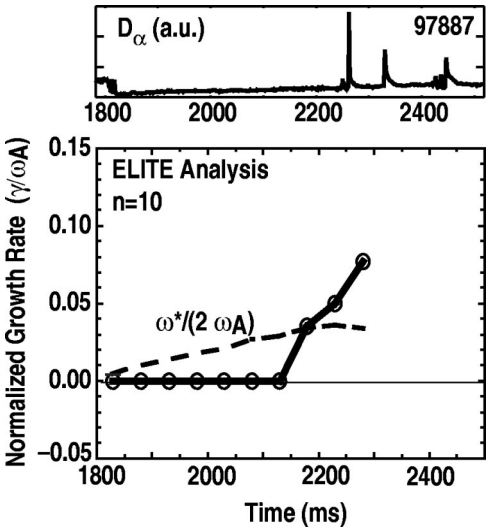

FIG. 6. Amplitude of the divertor D_α signal is shown above, indicating the $L-H$ transition and ELM times. Calculated $n=10$ normalized growth rate as a function of time is shown below, along with an estimate of the normalized $\omega_*/2$.

A. Case study: DIII-D shot 97887

In DIII-D VH-mode shot 97887, the $L-H$ mode transition at $t\sim 1810$ ms is followed by a long ELM free period, terminated by a large ELM at $t\sim 2240$ ms. To test the viability of peeling–ballooning modes as the ELM trigger, the growth rates of these modes are calculated with ELITE, using experimentally reconstructed equilibria at 50 ms intervals. Figure 6 shows the $n=10$ growth rate (γ) normalized to $\omega_A=v_A/R$, where v_A is the Alfvén speed. Intermediate n peeling–ballooning modes are found to go unstable at significant growth rates just before the first ELM is triggered. The value $n=10$ is chosen for the plot as it exhibits the largest value of γ/ω_*.

A further test is provided by comparing the calculated mode structure with the observed radial ELM depth. Figure 7(a) shows the measured relative electron temperature loss during an ELM ($\Delta T_e/T_e$), using normalized poloidal flux (ψ) as a radial coordinate. Good statistics are attained by taking the average loss profiles from Thomson scattering, for the two large ELMs occurring in the interval 2200 ms$<t<$2400 ms. The $n=10$ radial eigenmode structure calculated just before the first large ELM ($t=2230$ ms), is shown in Fig. 7(b). The measured ELM depth (for example, using full width at half maximum) and predicted mode depth agree, as predicted by the ELM model. Both extend significantly beyond the pedestal width ($0.95<\psi<1$). The 2D structure of the MHD radial displacement is shown in the contour plot inset in Fig. 7(b).

Additional confirmation of the predicted ballooninglike mode structure is provided by results from divertor balance experiments on DIII-D.[28] It is found that ELM energy deposited to the inner divertor leg becomes negligible in a double

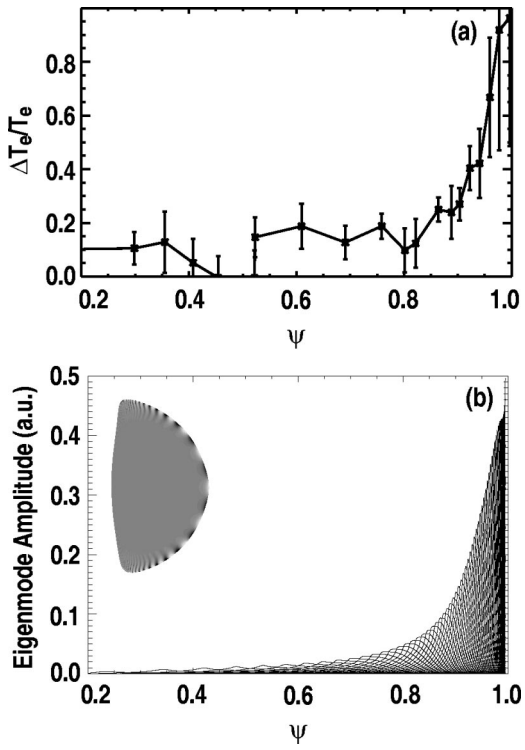

FIG. 7. (a) The observed radial profile of relative electron temperature loss across an ELM. (b) Radial profile of the calculated $n=10$ eigenfunction, just before the first ELM is triggered. The inset is a contour plot showing the 2D structure of the MHD radial displacement.

null configuration, suggesting that the ELM is localized on the low field side of the discharge, in agreement with the calculated mode structure.

B. Comparisons with JT-60U and Alcator C-Mod

Further comparisons of the model with observed ELM characteristics and pedestal limits have been carried out on the JT-60U and Alcator C-Mod tokamaks. These comparisons have consisted largely of side by side comparisons of pedestal stability and mode structure in pairs of shots exhibiting different ELM behavior.

On JT-60U, a regime of small ''grassy'' or ''type II'' ELMs is observed at high q and high δ, while large ''giant'' ELMs are observed at lower q,δ.[29] ELITE calculations for $n=12$, using experimentally reconstructed equilibria during the ELMy period, find that both grassy and giant ELM cases are marginally stable to peeling–ballooning modes. Broad mode structures are found for giant ELMs, and narrower structures for grassy ELMs, in agreement with the ELM model.

Peeling–ballooning stability of ''Enhanced D_α'' (EDA), ELM-free, and ELMing Alcator C-Mod discharges has been studied with ELITE. Intermediate $5<n<50$ growth rates were found to increase strongly with edge current, and to be higher with broader mode structure in ELMy cases than in EDA or ELM free. Results appear to be consistent with our model of ELMs as intermediate-n peeling–ballooning modes, while edge oscillations in EDA mode appear not to be related to ideal MHD instability. Results are to be discussed in detail in Ref. 10.

VI. DIAMAGNETIC STABILIZATION

The ideal MHD model used in the preceding sections neglects finite Larmor radius (FLR) effects which can be significant in the pedestal. In particular, diamagnetic drift stabilization has been considered by several authors as a potentially important effect in the pedestal (see, for example, Refs. 30–33).

The diamagnetic drift (ω_*) is a strong candidate to impact peeling–ballooning stability in the pedestal, because the strong pedestal pressure gradient leads to ω_* values that can be comparable to ideal MHD growth rates in many cases, particularly at higher n. The analytic relation[34,35]

$$-\gamma_{\mathrm{MHD}}^2=\omega(\omega-\omega_{*i}), \tag{2}$$

where γ_{MHD} is the ideal growth rate, implies that the ideal MHD instability becomes stabilized when $\omega_{*i}/2>\gamma_{\mathrm{MHD}}$. Equation (2) neglects kinetic effects, and assumes a constant value for ω_{*i}. Hastie, Catto, and Ramos[32] have developed a formulation for treating the strong variation of ω_{*i} typical of the pedestal, and have found that strong variation of ω_{*i} diminishes its stabilizing effect.

An estimate of $\omega_*/2$ normalized to ω_A is plotted in Fig. 6. While there are significant uncertainties in both ω_* and γ, a model which predicts the ELM will appear when $\gamma>\omega_*/2$ appears to be consistent with observations.

Motivated by consideration of diamagnetic stabilization, we designate the mode with the largest value of γ/ω_* (or equivalently, γ/n for a given equilibrium) as the most unstable mode for the purposes of our ELM model. Incorporating nonlocal ω_* effects into ELITE self-consistently is an important direction for future work.

VII. SUMMARY

ELMs can limit tokamak performance both directly, via large transient heat loads to divertor plates, and indirectly, through constraints placed on the edge pedestal height which impact global confinement. Hence a quantitative and predictive understanding of ELM physics is needed to reliably design next step fusion devices with both a high pedestal and tolerable ELMs.

The sharp pressure gradients in the H-mode transport barrier drive large bootstrap currents, and the combination of large p' and j provides drive for a variety of MHD instabilities over a wide range of toroidal mode numbers (n). The current plays a complex dual role in the pedestal, on the one hand, driving peeling instabilities, while on the other hand reducing shear and providing second stability access to ballooning modes. The picture is further complicated by the destabilizing coupling of peeling and ballooning modes which occurs at finite n.

A highly efficient, new MHD stability code, ELITE, has been developed to allow broad, quantitative study of MHD limits imposed on the pedestal over a wide range of $n>\sim 5$. ELITE has been used to explore the limits imposed both on pedestal pressure gradient, and through the collision-

ality dependence of the pedestal current, on the pedestal temperature itself. We find that the limiting instability is generally a peeling–ballooning mode of intermediate mode number ($3<n<30$).

We propose a model of ELMs in which peeling–ballooning modes provide the trigger, and the radial depth of the ELM correlates with the radial structure of the most unstable mode. The ELM size is proposed to correlate both with the radial mode structure, and with the location of the stability boundary in the pedestal parameter space. Qualitative ELM cycle models are also proposed to explain the observed ELM types which occur at high power.

Comparisons with experiment find that the calculated stability limits are consistent with observations. A case study with a DIII-D *VH*-mode structure finds that the first ELM is triggered just after peeling–ballooning growth rates achieve significant values, and the observed ELM depth is in good agreement with the calculated mode structure of the most unstable mode.

Diamagnetic stabilization is expected to contribute to pedestal stability, particularly at high n. The impact of ω_* is approximated by choosing the mode with largest γ/ω_* as the most unstable, and comparing values of γ and $\omega_*/2$. Incorporating diamagnetic effects into ELITE self-consistently is an important piece of future work.

While a great deal can be learned about ELMs and pedestal physics from linear stability analysis, nonlinear simulations, and incorporation of peeling–ballooning based ELM models into transport simulations are needed to develop fully quantitative descriptions of the complex dynamics of the ELM and pedestal dynamics, and these represent a critical direction for future work and further elaboration of our model of ELMs and constraints on the pedestal.

ACKNOWLEDGMENTS

The authors gratefully acknowledge contributions from Dr. M. S. Chu, Dr. J. W. Connor, Dr. G. T. A. Huysmans, Dr. R. L. Miller, Dr. T. W. Petrie, and Dr. M. R. Wade.

This work was funded by the U.S. Department of Energy under Grant No. DE-FG03-95ER54309, and by the UK Dept. of Trade and Industry and Euratom.

[1] H. Zohm, Plasma Phys. Controlled Fusion **38**, 105 (1996).
[2] W. Suttrop, Plasma Phys. Controlled Fusion **42**, A1 (2000).
[3] J. W. Connor, Plasma Phys. Controlled Fusion **40**, 191 (1998).
[4] L. L. Lao, Plasma Phys. Controlled Fusion **42**, A51 (2000).
[5] P. B. Snyder and H. R. Wilson, ''ELMs and the role of current-driven instabilities in the pedestal,'' Contrib. Plasma Phys. (to be published).
[6] A. E. Hubbard, Plasma Phys. Controlled Fusion **42**, A15 (2000).
[7] T. Hatae, M. Sugihara, A. E. Hubbard *et al.*, Nucl. Fusion **41**, 285 (2001).
[8] T. H. Osborne, J. R. Ferron, R. J. Groebner *et al.*, Plasma Phys. Controlled Fusion **42**, A175 (2000).
[9] J. R. Ferron, M. S. Chu, G. L. Jackson *et al.*, Phys. Plasmas **7**, 1976 (2000).
[10] D. Mossessian, P. B. Snyder, M. Greenwald, J. W. Hughes, Y. Lin, A. Mazurenko, S. Medvedev, H. R. Wilson, and S. Wolfe, ''*H*-mode pedestal characteristics and MHD stability of the edge plasma in Alcator C-Mod,'' Plasma Phys. Controlled Fusion (to be published).
[11] J. L. Luxon and L. G. Davis, Fusion Technol. **8**, 441 (1985).
[12] E. A. Frieman, J. M. Greene, J. L. Johnson, and K. E. Weimer, Phys. Fluids **16**, 1108 (1973).
[13] D. Lortz, Nucl. Fusion **15**, 49 (1975).
[14] J. A. Wesson, Nucl. Fusion **18**, 87 (1978).
[15] J. W. Connor, R. J. Hastie, H. R. Wilson, and R. L. Miller, Phys. Plasmas **5**, 2687 (1998).
[16] C. Mercier, Nucl. Fusion **1**, 47 (1960); Nucl. Fusion Suppl. **2**, 801 (1962).
[17] C. C. Hegna, J. W. Connor, R. J. Hastie, and H. R. Wilson, Phys. Plasmas **3**, 584 (1996).
[18] H. R. Wilson, J. W. Connor, A. R. Field, S. J. Fielding, R. L. Miller, L. L. Lao, J. R. Ferron, and A. D. Turnbull, Phys. Plasmas **6**, 1925 (1999).
[19] H. R. Wilson and R. L. Miller, Phys. Plasmas **6**, 873 (1999).
[20] P. B. Snyder, H. R. Wilson, X. Q. Xu, J. R. Ferron, L. L. Lao, M. S. Chu, E. J. Strait, and A. D. Turnbull, Europhys. Conf. Abstr. **24B**, 324 (2000).
[21] J. W. Connor, R. J. Hastie, and J. B. Taylor, Phys. Rev. Lett. **40**, 396 (1978).
[22] H. R. Wilson, P. B. Snyder, G. T. A. Huysmans, and R. L. Miller, Phys. Plasmas **9**, 1277 (2002).
[23] A. B. Mikhailovskii, G. T. A. Huysmans, S. E. Sharapov, and W. Kerner, Plasma Phys. Rep. **23**, 844 (1997).
[24] L.C. Bernard, F. J. Helton, and R. W. Moore, Comput. Phys. Commun. **24**, 377 (1981).
[25] M. Keilhacker and the JET Team, Plasma Phys. Controlled Fusion **41**, B1 (1999).
[26] H. Shirai and the JT-60 Team, Phys. Plasmas **5**, 1712 (1998).
[27] I. H. Hutchinson, R. Boivin, F. Bombarda *et al.*, Phys. Plasmas **1**, 1511 (1994).
[28] T. W. Petrie, J. G. Watkins, L. L. Lao, and P. B. Snyder, ''The role of magnetic balance on the poloidal distribution of ELM-induced peak particle flux at the divertor targets,'' Phys. Rev. Lett. (to be submitted).
[29] L. L. Lao, Y. Kamada, T. Oikawa *et al.*, Nucl. Fusion **41**, 295 (2001).
[30] T. S. Hahm and P. H. Diamond, Phys. Fluids **30**, 133 (1987).
[31] B. N. Rogers and J. F. Drake, Phys. Plasmas **6**, 2797 (1999).
[32] R. J. Hastie, P. J. Catto, and J. J. Ramos, Phys. Plasmas **7**, 4561 (2000).
[33] G. T. A. Huysmans, S. E. Sharapov, A. B. Mikhailovskii, and W. Kerner, Phys. Plasmas **8**, 4292 (2001).
[34] K. V. Roberts and J. B. Taylor, Phys. Rev. Lett. **8**, 197 (1962).
[35] W. M. Tang, R. L. Dewar, and J. Manickam, Nucl. Fusion **22**, 1079 (1982).